Journal of the European Ceramic Society **17** (1997) 1185–1192

PII: S0955-2219(96)00234-8
0955-2219/97/$17.00

The Effect of Reservoir Geometry on the Flow Within Ceramic Tape Casters

P. H. Gaskell,[a] B. Rand,[b] J. L. Summers[a] and H. M. Thompson[a]

[a]Department of Mechanical Engineering, [b]Department of Material Science, University of Leeds, Leeds, LS2 9JT, UK

(Received 22 July 1996; revised version received 7 November 1996; accepted 11 November 1996)

Abstract

The flow structure in the reservoir of a ceramic tape casting head is examined using a linear finite element formulation of the governing fluid mechanical equations, written in terms of the streamfunction and vorticity. Streamline plots are presented for representative reservoir shapes and depth-to-width (aspect) ratios.

Analysis predicts that the flow is characterised by an ever-present primary recirculation, adjacent to the moving web, and that the size and number of secondary recirculations above the primary one depend upon both the aspect ratio of the reservoir and the angle of inclination of the side walls. In particular, it is shown that the number of recirculations spanning the entire width of the reservoir increases at critical values of the aspect ratio, when eddies emanating from the upper corners merge together. The analysis also shows that for a given reservoir depth, it is possible to postpone the development of these secondary recirculations by 'opening out' the casting head, i.e. making the sides further away from the vertical, which may be a useful control mechanism for the design of such systems. © 1997 Elsevier Science Limited.

1 Introduction

Flat, thin ceramic layers are used widely in industry as a starting point for numerous ceramic products including thin capacitors, piezoelectric and electrostrictive monolayers, electronic substrates and multi-layer components.[1] These layers may be produced using a number of rival technologies including dry pressing, slip casting, extrusion/extrusion plus calendering, dry powder compaction, screen printing, electrophoretic deposition and tape casting.[2,3] However, it is the last process, illustrated in Fig. 1, that is of interest here. Tape casting is a relatively new process first used for the production of ceramic sheet capacitors in the 1940s[4] and is now an accepted precision coating method for the production of high-tech ceramic components. Tape casting can operate at speeds of up to several metres per minute and, of all the technologies listed above, it offers the widest range of layer thicknesses (from 20 to several hundred microns) and the thinnest self-supporting layers.[5]

Figure 1 is a schematic of a commonly encountered tape casting configuration. It consists of a reservoir bounded by rigid side walls and the slurry contained therein, while open at the top can escape from beneath a small gap, height H_c and accompanying doctor blade located at the lower edge of either the leading (as shown here) or trailing side-wall. The tape caster is mounted in contact with a flexible web (plastic substrate or steel belt) which forms the lower boundary of the system. Accordingly, relative motion between the reservoir and web can be produced in one of two ways: by pulling the web horizontally (continuous casting) with the casting head fixed (see Fig. 1) which is the usual mode of operation in the manufacture of large quantities of tapes, or by moving the casting head relative to a fixed web (discontinuous casting) typical of laboratory scale systems.

Few analyses of tape casting, reported in the literature, have been concerned with understanding its fundamental fluid mechanical behaviour[1] and most of these have tended to concentrate on understanding the influence of various casting parameters on the thickness and uniformity of the deposited layer.[6–8] However, in the context of industrial coating processes, Clarke[9] and Gaskell *et al.*[10] have noted that flow structure within coating/casting heads can have important implications for the quality of the final coated product. Consequently, in tape casting it is also important to

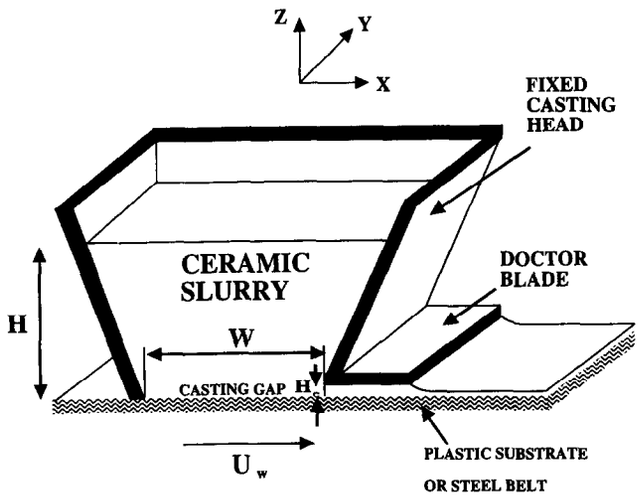

Fig. 1. Schematic of the ceramic tape casting process.

understand how the flow structure in the slurry reservoir is influenced by the casting head geometry and operating conditions since the presence of strongly recirculating flow can lead to inhomogeneities in the slurry. For example, bubbles and/or particulate contaminants may build up in these recirculations and, when subsequently released, may become trapped under the doctor blade, leading to non-uniformities such as 'streaks' in the deposited layer.

Recent work by Loest *et al.*,[11] for a specific case of a viscoplastic slurry and a relatively large casting gap (cf. Fig. 1), focused on the flow into an extended doctor blade region as well as the exit region where a free surface (meniscus) forms. The current work, however, is concerned with analysing flow in the slurry reservoir itself in the more usual situation of a *small* casting gap. In order to analyse the flow in the reservoir a simple model for its motion is formulated for arbitrary combinations of casting head side wall inclination and reservoir depth under the assumption of Newtonian flow behaviour. While in practice, of course, ceramic slurries can have widely different rheologies,[1,12] ranging from pseudoplastic (shear-thinning) and dilatant (thickening) to viscoplastic and fully viscoelastic, the first is the most commonly occurring[13] and predictions for the Newtonian case can still provide valuable information for pseudoplastic flows.[14] The model leads to a boundary value problem (bvp) which can be solved analytically for the special case with vertical side walls,[15] but the general case of non-vertical side walls is solved using a finite element technique. The results show that recirculating flow in the reservoir is inevitable adjacent to the web but that both the reservoir aspect ratio, i.e. the ratio of reservoir height, H, to width, W, and side wall inclinations are key factors in determining the flow structure.

2 Analysis

2.1 Governing equations

In the following analysis it is assumed that the flow is steady and isothermal and that the ceramic slurry behaves as an incompressible, Newtonian fluid. If, in addition, the casting head is sufficiently long in one particular direction (Y) so that the flow is essentially two-dimensional in a cross-sectional (X, Z) plane, the flow is governed by the two-dimensional momentum (Navier–Stokes) and continuity equations

$$\left.\begin{aligned} \rho \underline{U} \cdot \nabla \underline{U} &= -\nabla P + \eta \nabla^2 \underline{U} \\ 0 &= \nabla \cdot \underline{U} \end{aligned}\right\}, \tag{1}$$

where $\underline{U} = (U_x, U_z)$ is the two-dimensional velocity field, P is the modified pressure,[16] modified to take account of gravitational forces, and ρ and η are the slurry density and viscosity respectively. In theoretical fluid mechanics, it is usual practice to non-dimensionalise the velocity and pressure fields with respect to typical velocity and pressure scalings. If U^* and L^* are suitable velocity and length scales for the flow, it is convenient to introduce non-dimensional coordinates $x = X/L^*$, $z = Z/L^*$, velocities $\underline{u} = \underline{U}/U^*$ and modified pressures $p = PL^*/\eta U^*$ which allows eqns (1) to be rewritten as

$$\left.\begin{aligned} Re\, \underline{u} \cdot \nabla \underline{u} &= -\nabla p + \nabla^2 \underline{u} \\ 0 &= \nabla \cdot \underline{u} \end{aligned}\right\}, \tag{2}$$

where $Re = \rho U^* L^*/\eta$ is the Reynolds number measuring the relative importance of inertia to viscous forces. In most practical tape casting applications Re is at most O(1)[1,8,11] and it is, therefore, a reasonable simplification to adopt the 'Stokes' flow approximation of neglecting inertial effects altogether. This is equivalent to setting $Re = 0$ on the left hand side of eqn (2) as a result of which it is possible to formulate the equations of motion in terms of a *streamfunction* ψ, where $u_x = \partial\psi/\partial z$, $u_z = -\partial\psi/\partial x$ which automatically satisfies the continuity equation. In Stokes flow the momentum equation can be recast in terms of the biharmonic equation for the streamfunction.[16]

$$\nabla^4 \psi = 0. \tag{3}$$

In the numerical technique adopted here, it is convenient to reformulate eqn (3) in terms of the vorticity ω, in which case the biharmonic equation becomes

$$\left.\begin{aligned} \omega &= -\nabla^2 \psi \\ \nabla^2 \omega &= 0 \end{aligned}\right\}. \tag{4}$$

3 Modelling Assumptions

The above assumptions of steady, two-dimensional Stokes flow is augmented with the following additional simplifications:

(i) the upper slurry–air interface is planar with the air adjacent to the slurry remaining at uniform pressure and with negligible viscosity so that the shear stress vanishes at the interface;
(ii) the mass outflow from the reservoir beneath the doctor blade is negligible compared to that already in the reservoir.

These assumptions require further comment. Strictly speaking, assumption (i) corresponds to a case of infinite surface tension. However, the close agreement between theoretical predictions based on this assumption and experimental flow visualisations reported by Canedo and Denson,[17] for flow in polymer processing equipment, and by Gaskell *et al.*[10] in roll coating applications, supports the validity of this assumption in practical applications. The second assumption is motivated by the fact that the ratio of reservoir height to casting height, H/H_c, is typically of the order of 100,[1] so that the fractional rate of mass transfer out of the reservoir should indeed be small. Effectively, this assumption allows the reservoir to be taken as closed and with steady flow therein.

Scaling lengths by $W/2$, the semi-width of the reservoir bottom, and velocities by U_w, the web speed, permits the model to be formulated in terms of the dimensionless bvp shown in Fig. 2 where $A = H/W$ is the cavity aspect ratio and θ_L, θ_R are the angles that the left and right walls make with the vertical respectively.

4 Numerical Solution — the Streamfunction-Vorticity Method

The numerical approach adopted here is based on a variational formulation of the Stokes flow

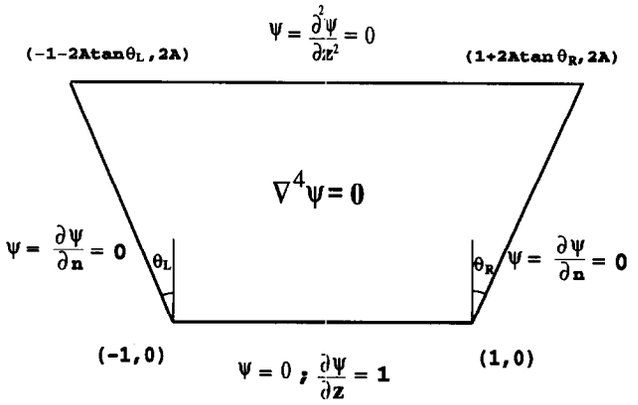

Fig. 2. Biharmonic bvp for idealised model of reservoir flow in a ceramic tape caster.

equations which are then discretised via the finite element (FE) method. Only the outstanding features of the method are described here; interested readers are referred to Gunzburger[18] for a description of FE methods in fluid mechanics and to Thompson[19] for a full exposition of the chosen 'streamfunction-vorticity' method.

It can be shown[19–21] that for closed domains Ω, with boundary $\partial\Omega$, for which ψ is constant on $\partial\Omega$ and for which the boundary conditions are simple combinations of either no-slip at a solid boundary or vanishing shear stress at a planar gas–liquid interface (as is the case in Fig. 2), eqns (4) are satisfied by those scalar fields ψ and ω that make the following functional

$$I(\psi, \omega) = \int_\Omega \left[-\nabla\psi \cdot \nabla\omega + \frac{\omega^2}{2} \right] d\Omega + \int_{\partial\Omega^1} V_t \omega ds. \quad (5)$$

stationary with respect to arbitrary variations in ψ and ω, where $\partial\Omega_1$ is the portion of the boundary over which no-slip conditions prevail and whose tangential velocity equals V_t.

The basic idea of the FE method is to tessellate the fluid domain into a number of contiguous elements, each with a number of nodes at which the values of ψ and ω are sought. Suppose, now, that the domain is tessellated into M such elements with N nodes and let N_k denote the interpolation function associated with the kth node. If $\bar{\psi}_k$ and $\bar{\omega}_k$ are the values of the streamfunction and vorticity at the kth node then their values at any point in the fluid are approximated by

$$\psi = \sum_{k=1}^{N} N_k \bar{\psi}_k \quad ; \quad \omega = \sum_{k=1}^{N} N_k \bar{\omega}_k, \quad (6)$$

respectively. Substituting these FE approximations into eqn (5) yields

$$I(\bar{\psi}_j, \bar{\omega}_j) = \sum_{j,k=1}^{N} \left\{ \int_\Omega \left(\frac{N_j N_k}{2} \bar{\omega}_j \bar{\omega}_k - \nabla N_j \cdot \nabla N_k \bar{\omega}_k \bar{\psi}_j \right) d\Omega \right\} + \sum_{j=1}^{N} \left\{ \int_{\partial\Omega} N_j V_t \bar{\omega}_j ds \right\}. \quad (7)$$

The FE equations are obtained by requiring stationarity of eqn (7) with respect to the *independent* nodal parameters $\bar{\psi}_j$, $\bar{\omega}_j$ yielding

$$\frac{\partial I}{\partial \bar{\omega}_j} = \sum_{k=1}^{N} \int_\Omega [N_j N_k \bar{\omega}_k - \nabla N_k \cdot \nabla N_k \bar{\psi}_k] d\Omega + \int_{\partial\Omega^1} N_j V_t ds = 0, \quad (8)$$

and

$$\frac{\partial I}{\partial \bar{\psi}_j} = \sum_{k=1}^{N} \int_\Omega \nabla N_j \cdot \nabla N_k \bar{\omega}_k d\Omega = 0. \quad (9)$$

Expressions (8) and (9) yield the required $2N$ algebraic equations for the unknowns $\bar{\psi}_k$ and $\bar{\omega}_k$ which, owing to their linear nature, can be obtained by a single matrix inversion. In the present work eqns (8) and (9) are solved using an efficient 'Frontal' solution method, originally due to Hood.[22]

4.1 Treatment of corner singularities

The conventional assumption of no-slip between liquid and solid surfaces loses its validity at both lower corners of the closed reservoir since the liquid velocity is undefined close to these points. In the numerical results reported here, the need for excessive grid refinement near these corners is removed by employing Moffatt's[23] theoretical results for flow in such corners to generate accurate boundary conditions on vorticity at the nodes closest to them. This technique has proved effective in the past for a wide range of different Stokes flow problems.[15,19–21]

5 Results

All numerical results reported here have been tested for grid independence by obtaining numerical solutions on three different grid levels and then checking that the solutions have converged with respect to the grid. A typical FE grid used in the numerical solutions is shown in Fig. 3; it consists of 544 elements and 1169 nodes.

To facilitate later comparison with results for more general situations, it is instructive to begin by reviewing the results reported by Gaskell *et al.*[15] for the special case with vertical side walls for which $\theta_L = \theta_R = 0°$. In this case the bvp shown in Fig. 2 can be solved analytically, while more general situations have to be solved numerically. Figures 4 and 5 show streamline patterns for reservoirs with aspect ratios in the range $A \in [0{\cdot}25, 5{\cdot}0]$. For $A \leq 1{\cdot}0$ each flow consists of a single primary recirculation pattern, symmetrical about the z axis, whose centre is closer to the moving web than to the slurry–air interface. As A increases beyond 1·0, eddies can be identified in the vicinity of the junctions between the side walls and the slurry–air interface which eventually merge to form a secondary eddy above the primary one at a critical aspect ratio $A_1^* \in (1{\cdot}61, 1{\cdot}62)$. This eddy creation mechanism and eddy growth, out from the upper reservoir corners, is repeated regularly as the aspect ratio is increased further. Figure 5 (c), for example, shows streamlines with $A = 5{\cdot}0$, for which the flow consists of three large recirculations and a smaller one adjacent to the slurry–air interface.

Figures 6 and 7 show how the flow structure is altered by setting $\theta_L = \theta_R = 15°$. For $A \leq 1{\cdot}0$ the flow is qualitatively similar to that observed for vertical side walls in that the flow consists of a single, large recirculation pattern with the eddy centre closer to the moving web than it is to the slurry–air interface. However, a slight difference between these flows is that for $\theta_L = \theta_R = 15°$ there are now small corner eddies at the junction between the side walls and the slurry–air

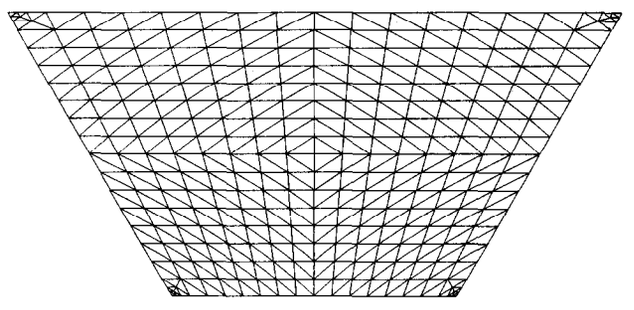

Fig. 3. A typical FE grid used in numerical solutions of the idealised model's bvp.

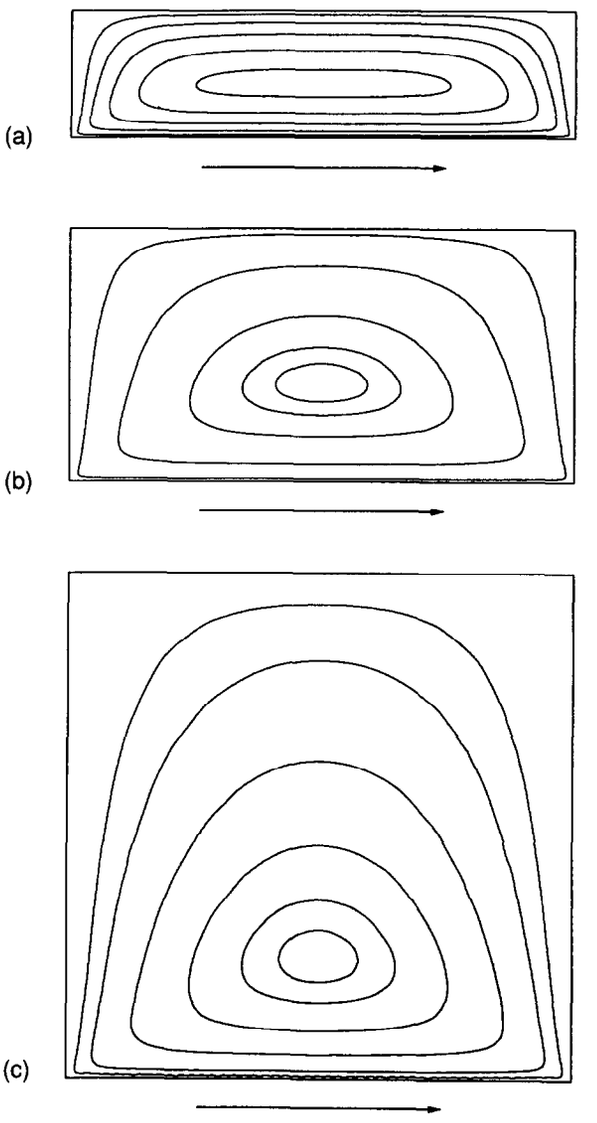

Fig. 4. Streamlines for the case $\theta_L = \theta_R = 0°$ with A = (a) 0·25, (b) 0·5, (c) 1·0.

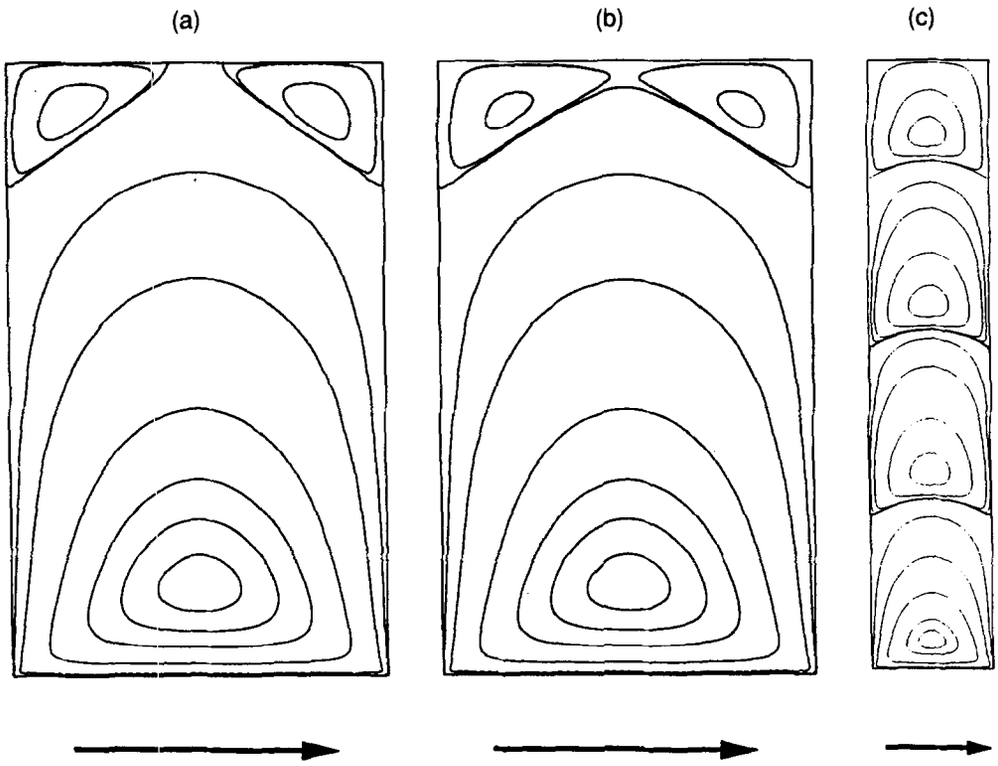

Fig. 5. Streamlines for the case $\theta_L = \theta_R = 0°$ with A = (a) 1·61, (b) 1·62 (c) 5·00.

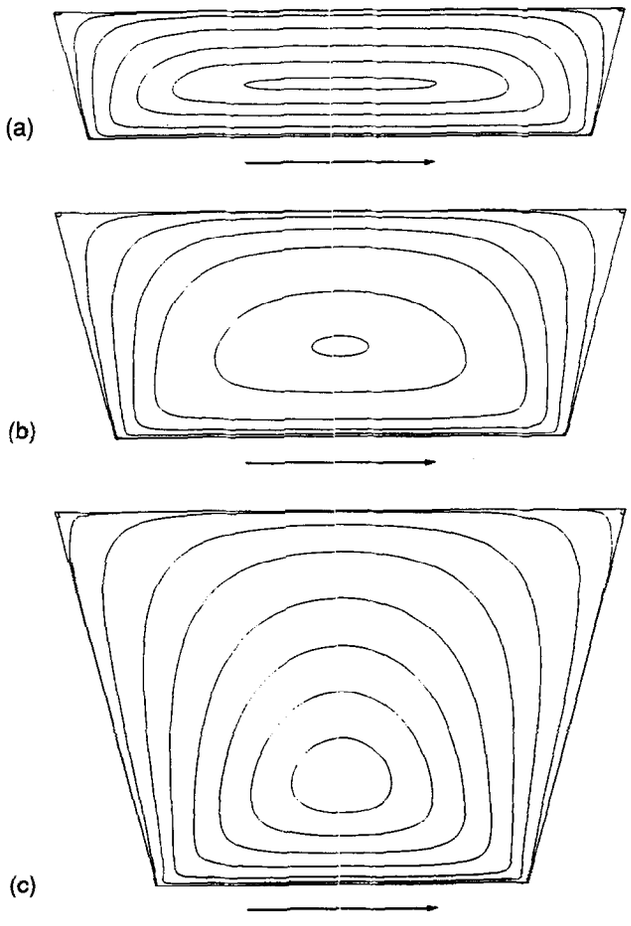

Fig. 6. Streamlines for the case $\theta_L = \theta_R = 15°$ with A = (a) 0·25, (b) 0·50 (c) 1·00.

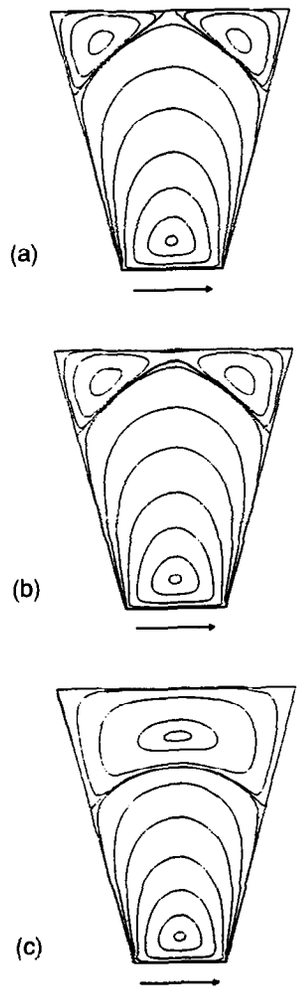

Fig. 7. Streamlines for the case $\theta_L = \theta_R = 15°$ with A = (a) 2·56, (b) 2·57 (c) 3·00.

interface. As A increases beyond 1·0 the corner eddies eventually grow until at a critical aspect ratio $A_1^* \in (2{\cdot}56, 2{\cdot}57)$ the corner eddies merge and form a secondary eddy structure above the primary one. Figures 8 and 9 show streamlines for $\theta_L = \theta_R = 30°$. For $A \leq 1{\cdot}0$ the flow is quantitatively similar to that for $\theta_L = \theta_R = 15°$, but now the critical aspect ratio $A_1^* \in (4{\cdot}65, 4{\cdot}66)$. Figure 10 examines the general trend that increasing θ_L and θ_R delays the merging of the corner eddies to form a secondary eddy structure above the primary one by showing the critical aspect ratio A_1^*, at which this merging occurs, as a function of $\theta = \theta_L = \theta_R$. (Note that negative θ refers to side walls being inclined inwards.) It can be seen that A_1^* increases rapidly as θ is taken above 30°.

Finally, Figs 11 and 12 show streamlines for the asymmetrical case where $\theta_L = 30°$ and $\theta_R = 15°$. Although for $A \leq 1{\cdot}0$ asymmetry only has a minor effect on the flow sufficiently far from the reservoir corners and, as predicted by Moffatt,[23] the relative size of the upper corner eddies is dependent on the wall inclinations. The asymmetry becomes more pronounced as the critical aspect ratio A_1^* is approached — the corner eddies adjacent to the left wall are larger than those adjacent to the right wall. Figure 12 (c) clearly shows the asymmetrical nature of the secondary eddy for $A = 4{\cdot}0$.

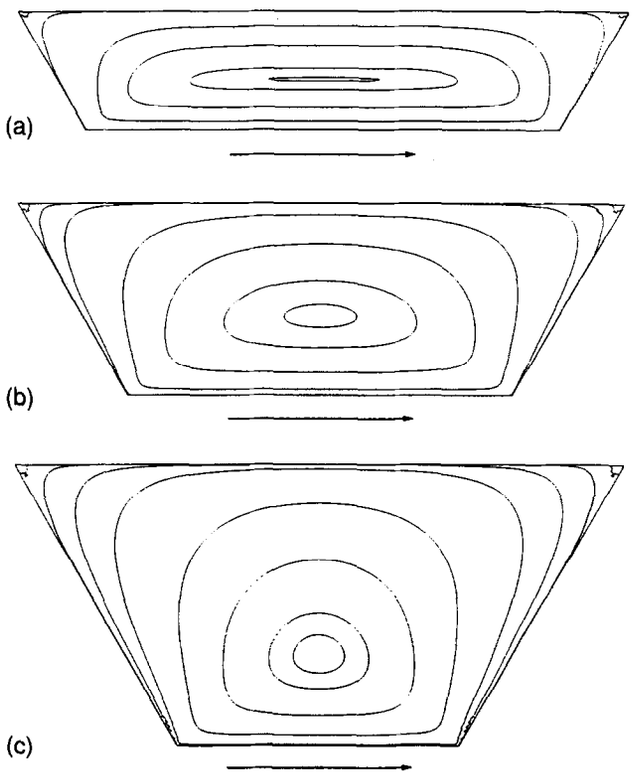

Fig. 8. Streamlines for the case $\theta_{KL} = \theta_R = 30°$ with A = (a) 0·25, (b) 0·50 (c) 1·00.

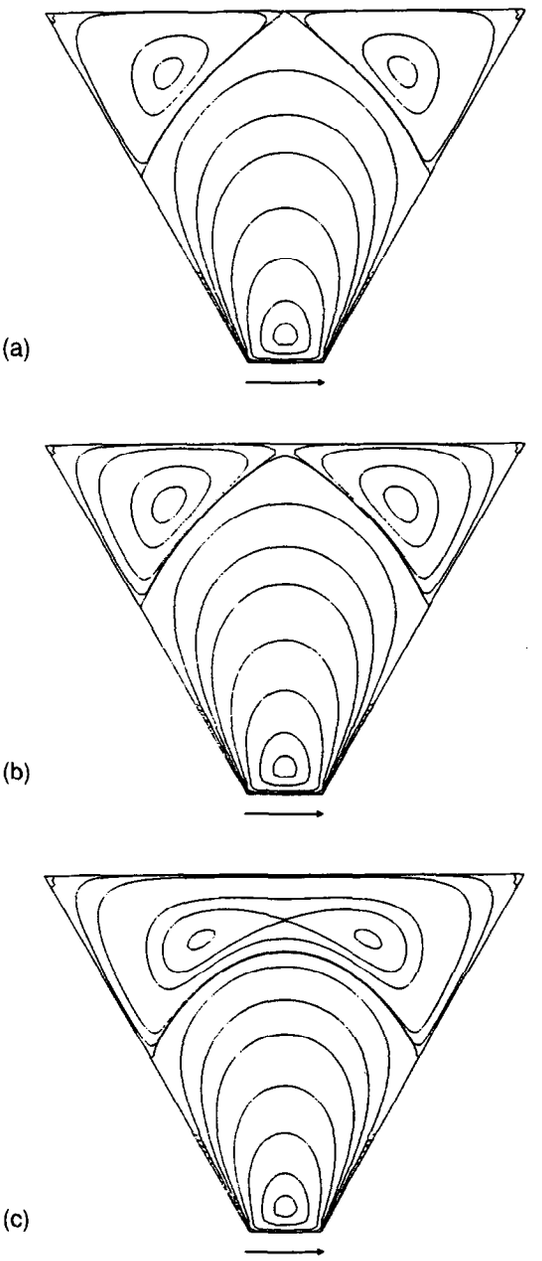

Fig. 9. Streamlines for the case $\theta_L = \theta_R = 30°$ with A = (a) 4·65, (b) 4·66 (c) 5·00.

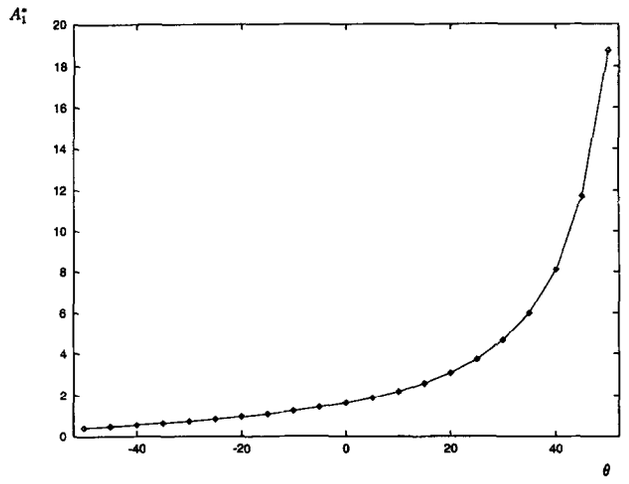

Fig. 10. Plot of critical aspect ratio A_1^* against $\theta = \theta_L = \theta_R$ for $-50° \leq \theta \leq 50°$.

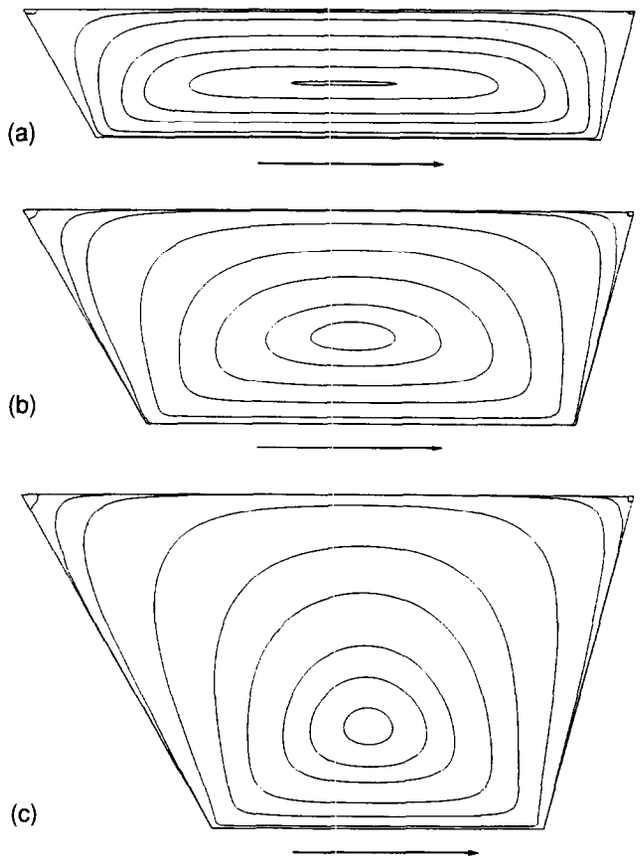

Fig. 11. Streamlines for the case $\theta_L = 30°$, $\theta_R = 15°$ with $A =$ (a) 0·25, (b) 0·50 (c) 1·00.

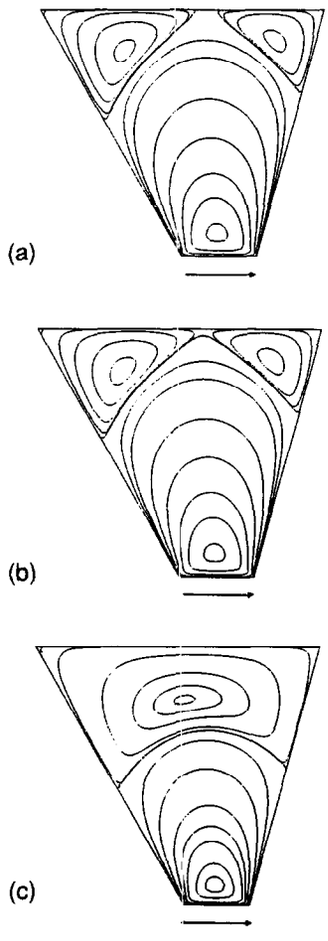

Fig. 12. Streamlines for the case $\theta_L = 30°$, $\theta_R = 15°$ with $A =$ (a) 3·33, (b) 3·34 (c) 4·00.

6 Conclusion

In this paper a simple model for flow in the reservoir of a tape caster has been developed whose predictions provide valuable insight into the flow structure and how it is influenced by the reservoir size and shape. Such information can be used to optimise casting head design so as to restrict the effects of recirculating flow as a possible cause of inhomogeneities and even defects in the deposited layer due to a build-up of bubbles and/or particulate contaminants.

The model predicts that although the existence of a *primary* recirculation, adjacent to the moving web, is inevitable the propensity for additional recirculations can be controlled by two key parameters: the cavity aspect ratio $A = H/W$ and the angle of inclination of the side walls. For a given casting head design the model predicts that the flow consists essentially of a primary recirculation provided A is below a critical value A_1^*; above A_1^* a large secondary eddy spanning the entire reservoir width also exists. The model predicts that A_1^* increases rapidly as the inclination angles θ_L, θ_R are increased. This feature may be useful if, for example, it is important to have a specific reservoir height in order to supply an adequate hydrodynamic head to assist flow through the casting gap (particularly important for larger doctor-blade gap clearances H_c[1]) since it is possible to postpone the onset of multiple recirculations simply by increasing θ_L and θ_R.

Clearly, the model developed here is only a first step towards understanding the fluid mechanics of the tape casting process. The model's predictions require a full experimental validation and the model needs to be extended to simulate more realistic rheological behaviour.[12,24–26] In addition to this modification the model should be extendable to include a small, finite outflux from the reservoir and also a full, numerical treatment of the free surface film flow of the cast tape after it has left the casting head.

References

1. Hellebrand, H., Tape Casting. In *Processing of Ceramics Part I*, ed. R. J. Brook. VCH Publishers, Wenheim, 1996.
2. Prasad, V.C.S., *Trans. Ind. Ceram. Soc.*, 1988, **41**, 85.
3. Fukuura, I. and Hirao, T. In *Advanced Technical Ceramics*, ed. S. Soniya. Academic Press, Tokyo, 1989, pp. 65–81.
4. Howatt, G. N., Breckenridge, R. G. and Brownlow, J. M., *J. Am. Ceram. Soc.*, 1947, **30**, 237.
5. Mistler, R. E. In *Engineering Materials Handbook, Vol. 4, Ceramics and Glasses*, ed. S. J. Schneider Jr., ASM International, Materials Park, OH, 1991.
6. Otsuka, K., Ohsawa, Y. and Yamada, K., *Yogyo Kyokai Shi*, 1986, **94**, 351.

7. Otsuka, K., Kitamura, W., Ohsawa, Y. and Sekibata, M., *Yogyo Kyokai Shi*, 1986, **94**, 1136.
8. Chou, Y. T., Ko, Y. T. and Yan, M. F., Fluid flow model for ceramic tape casting. *J. Am. Ceram. Soc.*, 1987, **70**(10), C280–C282.
9. Clarke, A., Recirculating flow in curtain coating. *Proc. First European Symposium Mechanics of Thin Film Coatings*, ed. P. H. Gaskell, M. D. Savage and J. L. Summers, pp. 32–41.
10. Gaskell, P. H., Savage, M. D., Summers, J. L. and Thompson, H. M., Modelling and analysis of meniscus roll coating. *J. Fluid Mech.*, 1985, **298**, 113–137.
11. Loest, H., Lipp, R. and Mitsoulis, E., Numerical flow simulation of viscoplastic slurries and design criteria for a tape casting unit. *J. Am. Ceram. Soc.*, 1994, **77**, 254–262.
12. Shaw, D. J., *Introduction to Colloid and Surface Chemistry*. London, Butterworths, 1975, pp. 187–205.
13. Dayton, G. O., Schulze, W. A., Shrout, T. R., Swartz, S. and Biggers, J. V., Fabrication of electromechanical transducer materials by tape casting. In *Advances in Ceramics*, ed. J. A. Mangels and G. L. Messing. 1984, vol. 9, pp. 115–139.
14. Coyle, D. J., Macosko, C. W. and Scriven, L. E., Film-splitting flows of shear-thinning liquids in forward roll coating. *AIChEJ*, 1987, **33**, 741–746.
15. Gaskell, P. H., Savage, M. D., Summers, J. L. and Thompson, H. M., Stokes flow in closed, rectangular cavities. *S.I.A.M. J. Appl. Math.*, submitted.
16. Batchelor, G. K., *An Introduction to Fluid Dynamics*. Cambridge University Press, Cambridge, 1994.
17. Canedo, E. L. and Denson, C. D., Flow in driven cavities with a free surface. *AIChEJ*, 1989, **35**, 129–138.
18. Gunzburger, M. D., *Finite Element Methods for Viscous Incompressible Flows*. Computer Science and Scientific Computing, Academic Press, San Diego, CA, 1989.
19. Thompson, H. M., A theoretical investigation of roll coating phenomena. PhD Thesis, Univ. of Leeds, UK, 1992.
20. Gaskell, P. H. and Mobbs, S. D. An efficient vorticity-streamfunction finite element method for viscous flow, 23rd *Brit. Theo. Mech. Coll. Leeds*, 1985.
21. Gaskell, P. H., Savage, M. D., Summers, J. L. and Thompson, H. M., Creeping flow analyses of free surface cavity flows. *Theoretical and Computational Fluid Dynamics*, 1996, **6**, 415–433.
22. Hood, P., Frontal solution program for unsymmetric matrices. *Int. J. Numer. Meth. Eng.*, 1976, **10**, 379–399.
23. Moffatt, H. K., Viscous and resistive eddies near a sharp corner. *J. Fluid Mech.*, 1964, **18**, 1.
24. Goodwin, J. W., Rheology of ceramic materials. *Am. Ceram. Soc. Bull.*, 1990, **69**, 1694.
25. Chartier, T. and Boch, P. Preparation of mullite ceramics by tape casting and reaction-sintering. In *Science of Ceramics*, ed. D. Taylor, Institute of Ceramics, Shelton, UK, 1988.
26. Hampton, J. H. D., Savage, S. B. and Drew, R. A. L., Experimental analysis and modeling of slip casting. *J. Am. Ceram. Soc.*, 1988, **71**, 1040.